AIAA Paper 99-1725, Proceedings of the 15th CEAS/AIAA Aerodynamic Decelerator Systems Technology Conference and Seminar, Toulouse, France (1999).

FLUID–STRUCTURE INTERACTION SIMULATION OF A CROSS PARACHUTE: COMPARISON OF NUMERICAL PREDICTIONS WITH WIND TUNNEL DATA

Keith Stein[†], Richard Benney[‡]
U.S. Army Soldier and Biological Chemical Command
Soldier Systems Center
Natick, Massachusetts 01760, USA

Tayfun Tezduyar[§]
Mechanical Engineering and Materials Science
Army HPC Research Center – Rice University
Houston, Texas 77005, USA

Vinay Kalro[¶]
Development Team – Fluent, Inc.
Evanston, Illinois 60201, USA

Jean Potvin[#]
Parks College Parachute Research Group
Department of Physics – Saint Louis University
St. Louis, Missouri 63156, USA

and

Timothy Bretl [**]
Swarthmore College
Swarthmore, Pennsylvania 19081, USA

ABSTRACT

The dynamics of parachutes involve a complex interaction between the parachute structure and the surrounding flow field. Accurate representation of parachute systems dynamics requires treatment of the problem as a fluid–structure interaction (FSI). Numerical simulations were performed for a series of cross parachute wind tunnel experiments conducted at Saint Louis University (SLU). These experiments are part of the New World Vistas Precision Aerial Delivery program being run jointly by the U.S. Air Force Office of Scientific Research and the U.S. Army Soldier and Biological Chemical Command (SBCCOM). The FSI model consisted of a 3D fluid dynamics (FD) solver using the stabilized space–time finite element method, a structural dynamics (SD) solver, and a method of coupling the FD and SD solvers. Preliminary fully coupled FSI simulations have been performed, and results have been obtained, which predict the coupled FD and SD behavior, to include drag histories, computed flow fields, computed structural behavior, and equilibrium geometries for the structure. Comparisons of these numerical results with experimental wind tunnel data for three cross–parachute models at three different wind speeds are presented.

INTRODUCTION

A collaborative research program between the U.S. Army Soldier and Biological Chemical Command (SSBCCOM) and SLU is exploring the potential of utilizing a cross–parachute system as an optional High Altitude Low Opening (HALO) resupply and/or humanitarian capability for the U.S. Department of Defense. The program seeks to demonstrate the use of a low–cost main cross canopy in a reefed configuration as the drogue for the majority of the system's descent. The system will transition from drogue to full–open main at a prescribed al-

[†] Aerospace Engineer

[‡] Aerospace Engineer, Senior Member

[§] James F. Barbour Professor in Engineering

[¶] Finite Element Specialist, Development Team

[#] Professor, Department of Physics, Associate Member

[**] Student, Department of Engineering

titude that is either triggered by a timer set by a digitized computed aerial release point (CARP) algorithm prior to deployment or triggered by a height sensor on board the system. The goal is to demonstrate a High–Speed Container Delivery System (HCDS) prototype with a A–22 container deployed from up to 25,000 feet AGL with up to 2,200 pounds. The full scale demonstration is planned for the summer of 2001 and will include being integrated with a new digitized onboard CARP algorithm and near real time wind measurements to examine the increased accuracy gained by HALO versus the currently utilized HAHO (High Altitude High Opening) systems for resupply.

As a starting point, a series of wind tunnel experiments are ongoing at SLU to determine the stability, shape, flow field, surface pressure distributions, overall drag and many other parameters associated with a wide range of reefed and fully open cross–canopy configurations.[1] In addition, these tunnel tests and ongoing concurrent drop tests will explore the potential of utilizing a cross–canopy system for low cost precision airdrop applications via onboard control. SD models are being developed to perform studies of potential systems such as these cross–canopy systems.[2,3] Cross canopies are relatively inexpensive to manufacture, which suggests great potential for "one–time–use" applications. This work seeks to explore the capabilities and limitations associated with a wide range of cross canopies through concurrent FSI simulations, tunnel tests, and drop tests.

A series of wind tunnel experiments on full–open–scaled cross parachutes with varying suspension line lengths have been conducted at SLU and experimental procedures and results have been reported in detail in a companion paper by Brocato et al.[4] The prototype scaled cross parachutes present unique challenges due to their size and associated large tunnel blockage. These tests are being simulated with unique airdrop system FSI high performance computer (HPC) models being developed by a collaborative team of researchers from SBCCOM and the Team for Advanced Flow Simulation and Modeling (T*AFSM) [http://www.mems.rice.edu/tafsm] at the Army High Performance Computing Research Center (AHPCRC).[5–8] This paper presents our initial first order validations of the FSI predictions.

This collaborative program will continue exploring various cross–system configurations and the potential of cross–canopy control in the tunnel with concurrent FSI simulations. The tests will expand from examining steady state configurations to exploring the most promising reefed configurations to the dynamics of various disreefing concepts. The goal is to gain confidence in the FSI predictions from the tunnel validation results and utilize these tools to predict the detailed performance characteristics of the full–scaled system concurrently with the experimental program.

PROBLEM SETUP

The numerical FSI simulations consist of three components: the SD solution, the FD solution, and the coupling between the SD and FD. Prior to performing the FSI simulations, we obtained near equilibrium conditions for both the SD and FD. Thus, the FSI simulation process consists of three main stages. Firstly, the SD model is generated from cut patterns of the wind tunnel parachute model and stand–alone simulations are performed using a static prescribed pressure distribution. The resulting geometry from the SD simulation is used as the initial geometry for the FSI simulation. Secondly, a static FD simulation is performed about the static SD geometry and the resulting fully developed flow field is used as the initial condition for the FSI simulation. Thirdly, the FSI model is set up and the FSI simulation is performed.

SD Model

Three cross parachute wind tunnel models are modeled. The experimental wind tunnel models are each composed of a canopy section which is constructed out of five one square foot panels of low porosity material, 20 suspension lines, reinforcements along the seams in the canopy, which extend from the suspension lines through the canopy, and reinforcements at the outer edges of the canopy between the suspension line attachment points. Each of the 20 suspension lines has the same length with values of 50 inches, 45 inches, and 40 inches for the three cases. The SD model approximates the canopy portion of the parachute using 9–noded membrane elements. The suspension lines and reinforcements are represented with 2–noded cable elements. The composition of the base parachute model (with 50–inch suspension lines) is shown in a "blown–out" view in Figure 1 where the lower set of lines represents the suspension lines, the middle section represents the cross canopy, and the upper set of lines represents the reinforcements in the canopy along the seams and outer edges. The inner three suspension lines for each arm of the cross parachute are constructed in a kinked configuration (as depicted in Figure 1) in order that each of the suspension lines has the identical unstretched length of 50 inches.

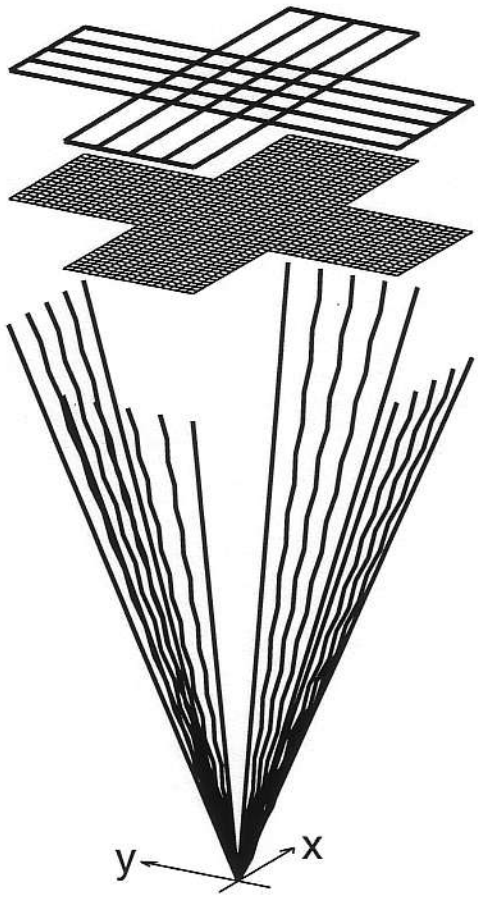

Figure 1. Cross parachute constructed configuration.

The base wind tunnel model has a total weight of approximately 0.50 pounds. The suspension lines, canopy, and reinforcements assume approximately 0.23, 0.06, and 0.21 pounds of the total weight respectively. The material properties for the SD model are shown in Table 1. These values are taken as representative of the wind tunnel model. Material densities are defined based on the assumed membrane thickness and cable areas to satisfy the known weight requirement for the cross parachute. Linear–elastic material stiffnesses are defined to result in membrane and cable strains of approximately one percent for the inflated configuration. Thus, the selected values for membrane and cable Young's modulus are approximate, but representative of the cross–parachute model.

The base SD model mesh consists of 5,694 nodes, 1,280 nine–noded membrane elements for the canopy surface, and 1,488 two–noded cable elements for the suspension lines and canopy reinforcements. The suspension lines connect to a single confluence point, which represents the fixed attachment point in the wind tunnel test section. This mesh results in 17,079 equations.

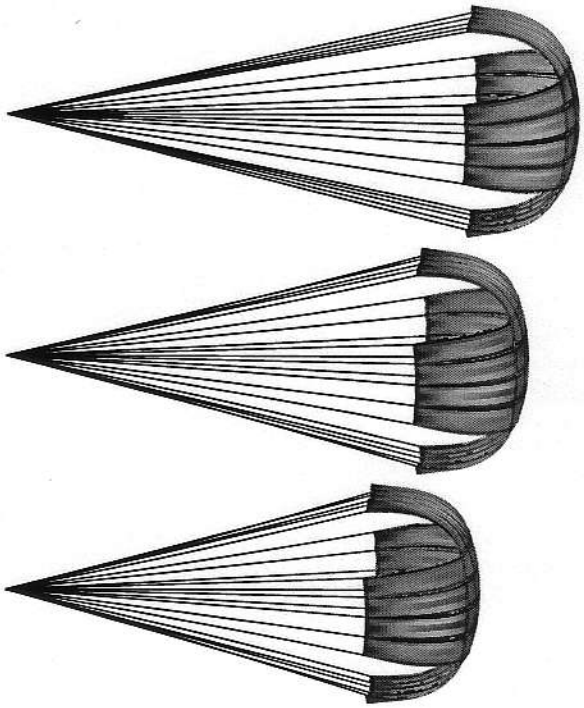

Figure 2. Fully inflated configurations for the cross–parachute models.

The base model is allowed to inflate when the canopy is subjected to a prescribed nondimensional differential pressure of 4.0 lb/ft^2. The fully inflated equilibrium configuration for the base model is obtained by a damped dynamic SD simulation and is shown in the top picture of Figure 2. Maximum principal stresses for the parachute canopy (membrane) are superimposed on the surface, with dark regions representing the low stresses (predominant along the canopy reinforcements) and light regions representing high stresses. This equilibrium solution is used to define the initial parachute canopy configuration in the FD model.

The SD mesh for the 50–inch suspension line base model is used to define the 45–inch and 40–inch SD models. This is accomplished by "pulling" the suspension lines by 5 and 10 inches in order to represent the 45–inch and 40–inch models, respectively. These line pulls are modeled by changing the natural lengths of the suspension line cables during a dynamic stand–alone SD simulation[2,8] . The internal stresses in the cables are computed based on the changing natural lengths. However, the inertial and gravitational terms are calculated based on the initial natural lengths for the cables. Thus, the total

mass of the SD models remains constant during the simulations. After the line pull, the 45–inch and 40–inch SD models are allowed to reach static equilibrium. These equilibrium conditions are used to define the initial conditions in the FD model. The static equilibrium configurations for the 50–inch, 45–inch, and 40–inch models are shown in Figure 2.

CFD Model

The FD model is developed to be representative of the SLU wind tunnel which has a (28 inch × 39 inch × 54 inch) test section, with the cross–parachute canopy as an interior boundary. For the FD model we extend the length of the test section to make sure that there will not be any reverse flow at the exit boundary, which would not be legal for our stress–free exit boundary condition. The numerical model consisting of the test section and parachute canopy is shown in Figure 3, with the dashed lines representing the diverging boundaries of the wind tunnel downstream from the test section. In order to discretize the volume included in the numerical model of Figure 3, we first generate an unstructured triangular surface mesh for the boundaries included in the model. For the canopy surface we generate the surface mesh for the inflated canopy by first generating a mesh for the flat canopy, and then projecting the displacements from the SD simulation onto the flat mesh. This process is depicted in Figure 4 with the flat surface mesh (upper left), the deformed SD canopy mesh with 9–noded membranes (upper right), and the deformed surface mesh (bottom). It should be noted that each panel in the canopy surface mesh was meshed separately in order to maintain a set of edges that define the reinforcements along the seams of the cross canopy. In addition to the outer boundaries and the canopy boundary in the FD model, a "refinement boundary" mesh is generated in the wake region of the canopy to control the level of refinement in this region. The refinement boundary is represented by the dotted lines in Figure 3.

The complete surface mesh for the FD model is shown in Figure 5. This surface mesh is used as input with automatic mesh generation software developed by the T*AFSM at the AHPCRC in order to generate a 3–D tetrahedral mesh of the FD domain. For this mesh, the canopy surface is split into unique upper and lower surfaces. This mesh generation process is performed for each of the SD models.

The FSI simulations use a stabilized space–time finite element formulation[9,10] of the time–dependent, 3–D Navier–Stokes equations of incompressible flows.

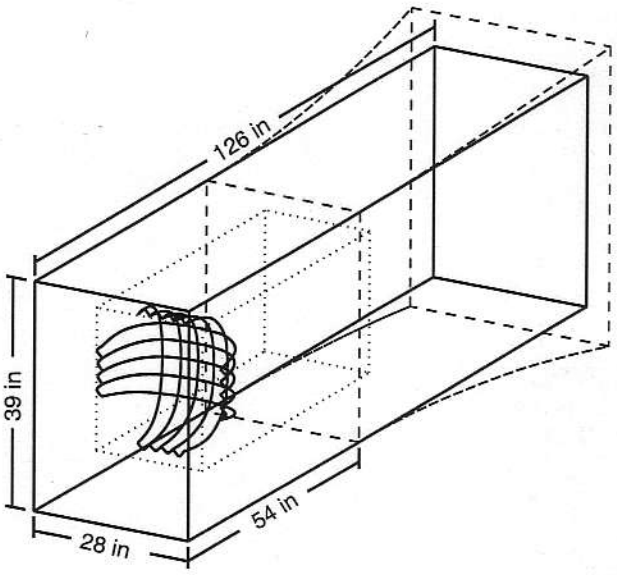

Figure 3. Cross parachute wind tunnel test: Numerical FD domain.

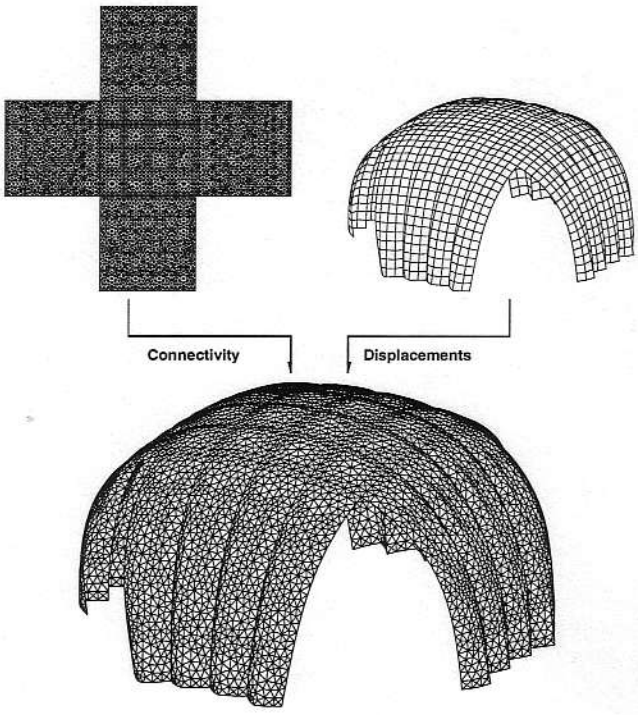

Figure 4. Cross–parachute canopy surface mesh.

In this formulation the finite element interpolations polynomials are functions of both space and time and the stabilized variational formulation of the problem is written over the associated space–time domain, automatically taking into account deformations in the spatial domain and protecting the computation against numerical oscillations. These meth-

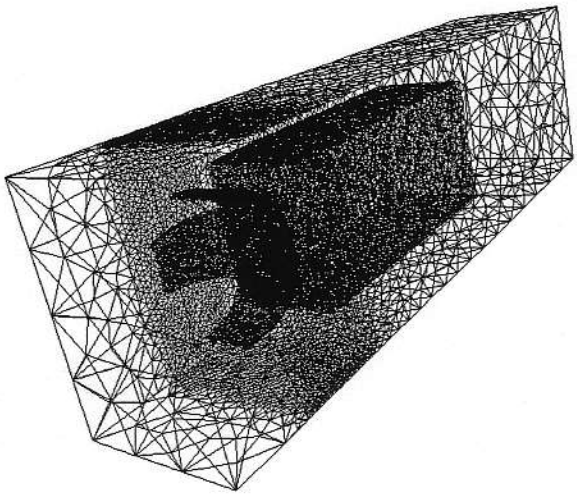

Figure 5. Cross parachute: Surface mesh of FD domain.

ods have been tested on a variety of problems involving deforming domains, to include parachute FSI problems.[6–8] We perform initial FD simulations about the fixed–canopy geometries in order to allow the flow field to develop prior to performing the FSI simulation. Since these stand–alone simulations are about fixed canopies, we use a stabilized "semi–discrete" formulation for the FD equations.[11] The semi–discrete formulation handles the temporal coordinate with finite differencing and thus is less computationally intensive than space–time formulations. However, the semi–discrete method is adequate for the stand–alone simulations since there is no time dependence in the spatial domain (i.e., no deformation of the canopy). After the flow has developed, we run the simulation for several timesteps with the stabilized space–time formulation to obtain a converged set of restart files for the FSI simulations, which utilize the space–time formulation to handle spatial deformations. Table 2 shows the mesh size and resulting number of equations for each of the FD meshes.

The boundary conditions for the FD simulations are imposed to approximate the conditions of the wind tunnel: the inflow boundary is prescribed to have a constant velocity of 40, 60, or 80 miles per hour, the side boundaries are prescribed to have zero normal velocity and no shear stress, and the outflow boundary is prescribed to be stress–free. In addition, a no–slip condition is imposed on the cross–parachute canopy surface. Simulations to develop the flow field are performed for each FD mesh and for inflow velocities of 40, 60, and 80 miles per hour.

FSI Coupling

FSI coupling occurs over the FD–SD interface, the cross–parachute canopy surface. In the simulations, it is assumed that the suspension lines have no effect on the flow field. Instead, simple line drag approximations are imposed as forces in the SD model. The cross canopy surface meshes for the FD and SD models are incompatible (i.e., nodally inequivalent, different element types), as depicted in Figure 4. Coupling information is transferred between the incompatible surface meshes by a least squares projection scheme.[8] Surface pressures from the FD solution are projected from the FD triangular surface mesh to the integration points of the 9–noded membrane elements in the SD mesh. Likewise, canopy surface displacements and velocites from the SD solution are projected from the SD to the FD mesh. The displacements are imposed as deformations in an automatic mesh moving scheme[12] in order to accurately represent the canopy surface in the FD mesh. The velocities are used to impose a noslip boundary conditions on the canopy surface in the FD simulation.

RESULTS

Average drag for the parachute calculated from the results of the FSI simulations are compared with experimental data from the SLU wind tunnel experiments and are summarized in Table 3. A comparison of these results is shown in Figures 6–9. Figures 6 and 7 show the comparison of the FSI–predicted drag with the wind tunnel drag measurements as a function of suspension line length for inflow velocities of 40 and 60 miles per hour. Figures 8 and 9 show the comparison of the FSI–predicted drag with the wind tunnel drag measurements as a function of inflow velocity for two cross–parachute models. Figure 8 corresponds to the cross–parachute model with 40 inch suspension lines. In Figure 9, the suspension line length for the FSI and wind tunnel models differ by one inch, with the FSI model having 50–inch lines and the wind tunnel model having 51–inch lines. These plots in Figures 6–9 show good agreements in the drag trends and have errors ranging from 3-10 percent.

A hot–wire probe was inserted into the wind tunnel for the 51–inch suspension line model and measurements were taken for the streamwise velocity component. These measurements were taken 16 inches downstream from the canopy–suspension line connection points and across the tunnel 39-inch width and in the vertical midplane of the tunnel test

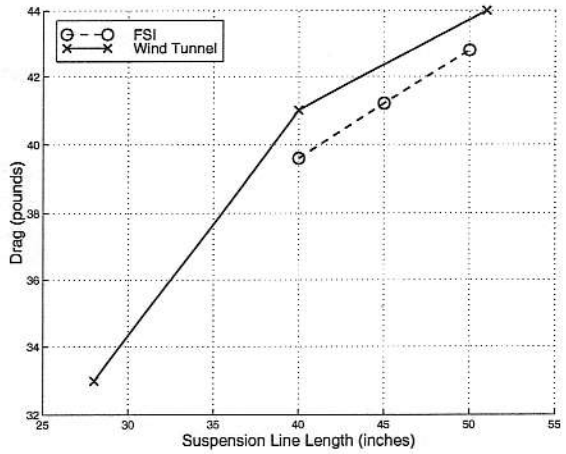

Figure 6. Drag comparison for 40 miles/hour inflow velocity.

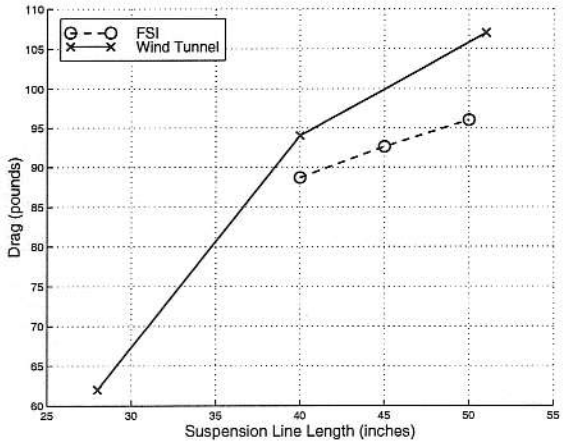

Figure 7. Drag comparison for 60 miles/hour inflow velocity.

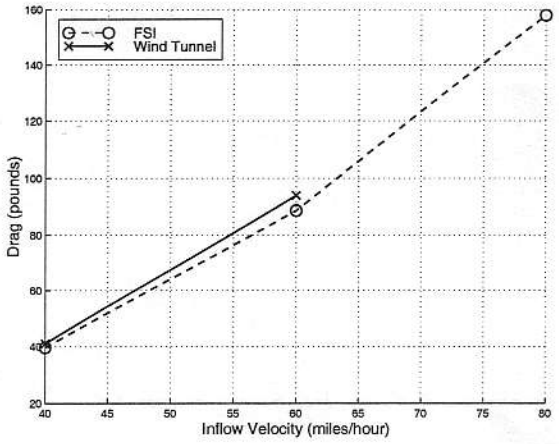

Figure 8. Drag comparison for 40–inch cross parachute.

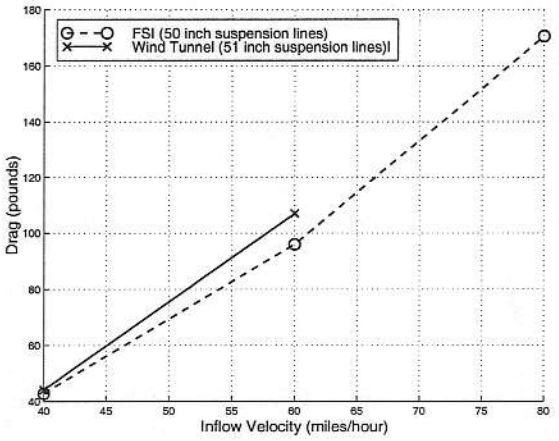

Figure 9. Drag comparison for 50–inch cross parachute.

section. Computed values for the velocity were averaged and are compared with the measured values in Figure 10.

Shape comparisons are made for the cross parachute with 50–inch suspension lines at a tunnel speeds of 40 and 60 miles per hour. Figure 11 shows the predicted configuration for the inflated canopy from the FSI simulation (left) and for the wind tunnel experiments (right) at 40 miles per hour. Measurements were made on the projected width of the center square panel in the cross–parachute canopy. Experimental measurements from video data showed projected widths of 11.5±0.3 and 11.2±0.3 inches for tunnel speed of 40 and 60 miles per hour respectively. Average computed values for the projected widths were approximately 11.7 inches for both tunnel speeds. The deviations between the FSI and experimental values are small and can most likely be attributed to a combination of FSI simulation approximations and experimental measurement errors. The computed average panel width for the FSI simulations are shown in Figure 12.

Several flow snapshots from the FSI simulation for the 50–inch suspension line model and with an inflow of 40 miles per hour are shown in Figures 13-15. These snapshots all correspond to the same instant in time. The figures show the nondimensional pressure ($\hat{p} = (p - p_\infty)/\rho U_\infty^2$) and velocity magnitude ($V = \frac{\|u\|}{U_\infty}$), where p_∞ and U_∞ are the pressure and velocity at the inflow boundary and ρ is the density of air. For each of the snapshots in Figures 13-15, $\Delta\hat{p}$ is 0.31 between pressure contours and ΔV is 0.25 between velocity contour lines. It should be noted in Figures 13 and 15 the cutting planes cut through the parachute canopy surface. Thus, the pressure

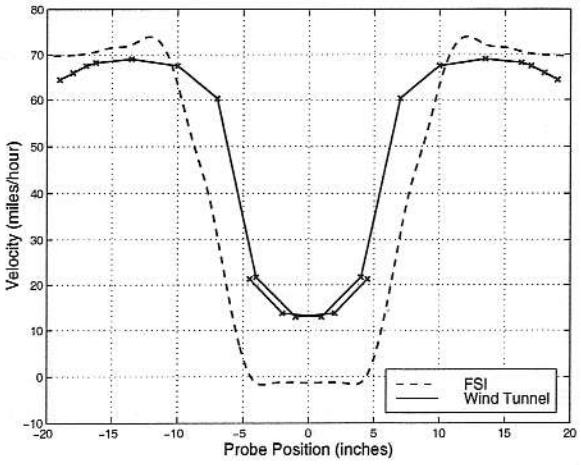

Figure 10. Comparison of the computed and measured streamwise velocity component.

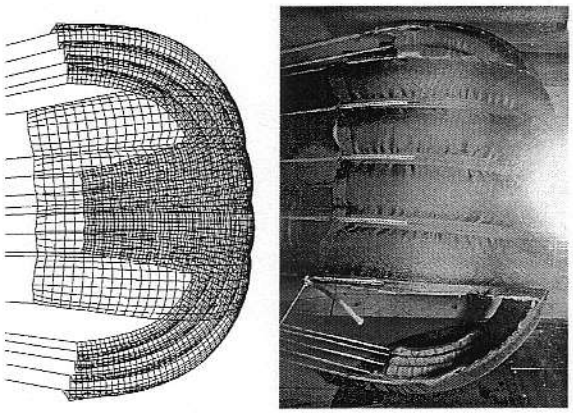

Figure 11. Cross parachute shape comparison.

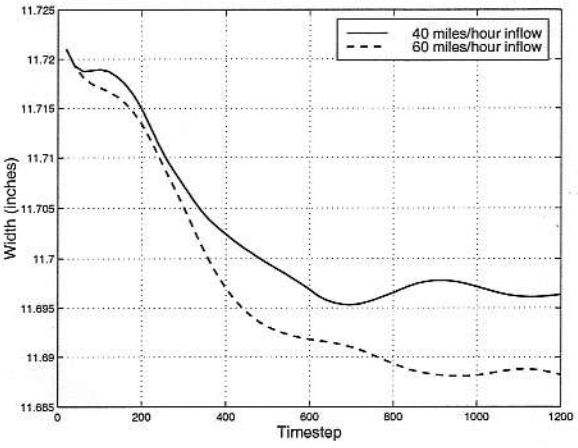

Figure 12. Predicted average panel width for 50–inch model.

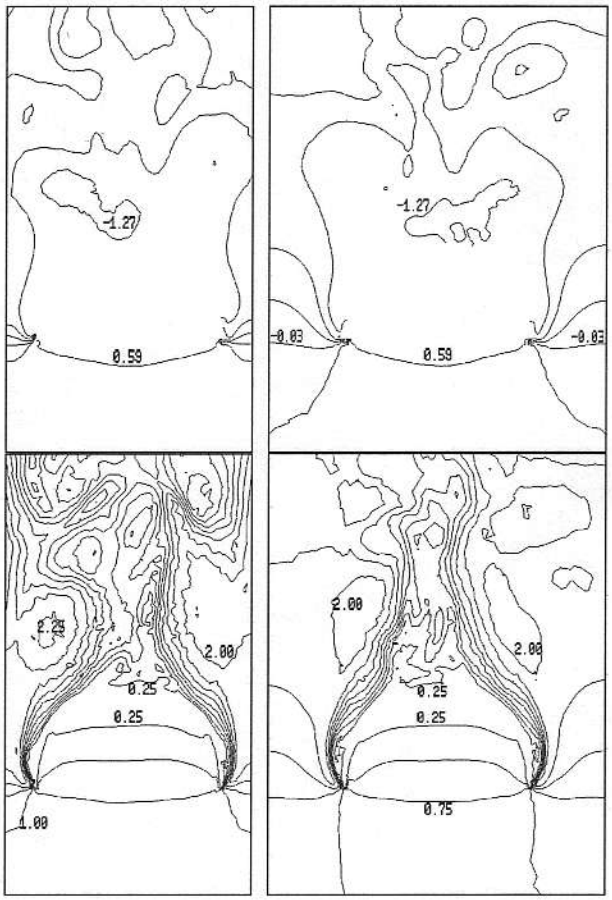

Figure 13. Pressure (top) and velocity magnitude (bottom) contours in cutting planes bisecting the tunnel.

contours end at the canopy surface since pressure is discontinuous across the surface.

Figure 13 shows $\hat{p}$ and V contours for the bisecting planes of the tunnel surrounding the cross parachute. The left figures correspond to the cutting plane across the 28–inch width of the tunnel and the right figures correspond to the cutting plane across the 39–inch height of the tunnel. Figure 14 shows the $\hat{p}$ and V contours on the tunnel walls surrounding the cross parachute. For the simulations, the wall boundary conditions was imposed to have zero normal velocity and no shear stress. It is apparent from the figures that the blockage effects are much more severe across the 28–inch test section width than across the 39–inch test section height. Figure 15 shows the $\hat{p}$ and V at two cutting planes normal to the inflow velocity. The left and right figures correspond to cutting planes 1.0 and 5.8 inches downstream from the canopy–suspension line connection points, respectively.

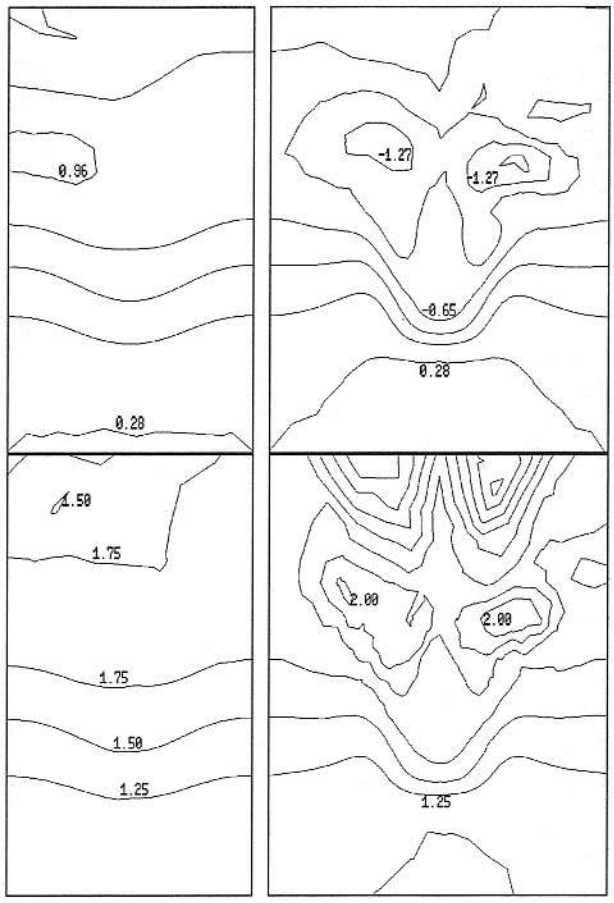

Figure 14. Pressure (top) and velocity magnitude (bottom) contours along tunnel walls.

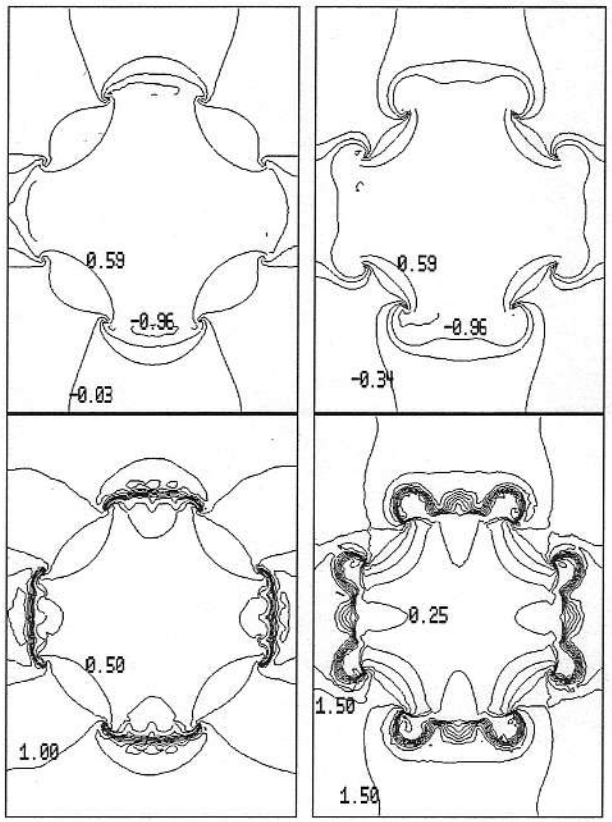

Figure 15. Pressure (top) and velocity magnitude (bottom) contours in normal cutting planes.

CONCLUSION

Preliminary FSI simulations have been performed to numerically model a series of wind tunnel experiments on cross parachutes conducted at SLU. Simulation results have been obtained and comparison have been made with experimental data. Initial comparisons on drag behavior, inflated shapes, and flow velocity profiles have been presented. The numerical model is being further refined to more accurately represent the physical experiments. This collaborative team is conducting further comparisons of FSI simulations with ongoing experiments.

ACKNOWLEDGMENTS

This work was sponsored in part by NASA–JSC (grant number NAG9–1059), by AFOSR (contract number F49620–98–1–0214), and by the Army HPC Research Center under the auspices of the Department of the Army, ARL cooperative agreement number DAAH04–95–2–0003 and contract number DAAH04–95–C–0008. The content does not necessarily reflect the position or the policy of the Government, and no official endorsement should be inferred.

References

[1] J. Potvin, L. Esteve, G. Peek, R. Alamat, and J. Little, "Wind Tunnel Study of Cruciform Parachutes Folded in Various Configurations", *Proceedings of the CEAS/AIAA 15th Aerodynamic Decelerator Systems Technology Conference*, AIAA-99-1739, Toulouse, France, 1999.

[2] R.J. Benney, K.R. Stein, J.W. Leonard and M.L. Accorsi, "Current 3-D Structural Dynamic Finite Element Modeling Capabilities", *Proceedings of the 14th AIAA Aerodynamic Decelerator Technology Conference*, AIAA-97-1506, San Francisco, 1997.

[3] R. Benney, K. Stein, w. Zhang, M. Accorsi, J. Leonard, "Controllable Airdrop Simulations Utilizing a 3–D Structural Dynamics Model", *Proceedings of the CEAS/AIAA 15th Aerodynamic Decelerator Systems Technology Conference*, AIAA-99-1727, Toulouse, France, 1999.

[4] B. Brocato, L. Esteve, D. Garcia, C. Manglano, G. Peek and J. Potvin, R. Benney and K. Stein, R. Alamat and J. Little, "Experimental Study of Fluid–Structure Interactions on a Cross Parachute: Comparison of Wind Tunnel Data and Drop Data with CFD Predictions", *Proceedings of the CEAS/AIAA 15th Aerodynamic Decelerator Systems Technology Conference*, AIAA-99-1737, Toulouse, France, 1999.

[5] R.J. Benney and K.R. Stein, "A Computational Fluid Structure Interaction Model for Parachute Inflation", *Journal of Aircraft*, **33** (1996) 730–736.

[6] K. Stein, R. Benney, V. Kalro, T. Tezduyar, J. Leonard, and M. Accorsi, "Parachute Fluid–Structure Interactions: 3–D Computation", ~~to appear in~~ *Computer Methods in Applied Mechanics and Engineering.* **190** (2000) 373-386.

[7] V. Kalro and T. Tezduyar, "A Parallel Finite Element Methodology for 3D Computation of Fluid–Structure Interactions in Airdrop Systems", *Proceedings of the 4th Japan-US Symposium on Finite Element Methods in Large-Scale Computational Fluid Dynamics*, Funabashi, Japan, 1998.

[8] K. Stein, R. Benney, V. Kalro, T. Tezduyar, J. Leonard, and M. Accorsi, "3–D Computation of Parachute Fluid–Structure Interactions: Performance and Control", *Proceedings of the CEAS/AIAA 15th Aerodynamic Decelerator Systems Technology Conference*, AIAA-99-1714, Toulouse, France, 1999.

[9] T.E. Tezduyar, M. Behr and J. Liou, "A new strategy for finite element computations involving moving boundaries and interfaces – the deforming-spatial-domain/space-time procedure: I. The concept and the preliminary tests", *Computer Methods in Applied Mechanics and Engineering*, **94** (1992) 339–351.

[10] T.E. Tezduyar, M. Behr, S. Mittal and J. Liou, "A new strategy for finite element computations involving moving boundaries and interfaces – the deforming-spatial-domain/space-time procedure: II. Computation of free-surface flows, two-liquid flows, and flows with drifting cylinders", *Computer Methods in Applied Mechanics and Engineering*, **94** (1992) 353–371.

[11] T.E. Tezduyar, "Stabilized Finite Element Formulations for Incompressible Flow Computations", *Advances in Applied Mechanics*, **28** (1991) 1-44. ← (1992)

[12] A.A. Johnson and T.E. Tezduyar, "Mesh Update Strategies in Parallel Finite Element Computations of Flow Problems with Moving Boundaries", *Computer Methods in Applied Mechanics and Engineering*, **119** (1994) 73–94.

Table 1. Cross parachute: Material properties.

	Membranes	**Cables**		
Material Group	Canopy	Suspension Lines	Seam Reinforcements	Edge Reinforcements
thickness (area)	0.0001 ft	(0.0001 ft^2)	(0.0001 ft^2)	(0.0001 ft^2)
density	3.75 slugs/ft^3	0.85 slugs/ft^3	2.0 slugs/ft^3	2.0 slugs/ft^3
Young's modulus	2.2×10^6 lb/ft^2	5.0×10^6 lb/ft^2	2.0×10^6 lb/ft^2	3.0×10^6 lb/ft^2
Poisson ratio	0.3	—	—	—

Table 2. Cross parachute tests: FD meshes.

SD Model (line length)	**number of nodes**	**number of elements**	**equations (semi–discrete)**	**equations (space–time)**
50 inches	129,121	774,129	481,529	963,058
45 inches	132,112	793,078	493,493	986,986
40 inches	133,456	802,013	498,869	997,738

Table 3. Cross parachute drag performance.

Simulation Number	**Cross Parachute Model**	**Tunnel Speed**	**Drag (FSI)**	**Drag (experiment)**
1	50–inch lines*	40 miles/hour	42.8 pounds	44.0 pounds
2	50–inch lines*	60 miles/hour	96.0 pounds	107.0 pounds
3	50–inch lines	80 miles/hour	170.5 pounds	– –
4	45–inch lines	40 miles/hour	41.2 pounds	– –
5	45–inch lines	60 miles/hour	92.6 pounds	– –
6	45–inch lines	80 miles/hour	164.5 pounds	– –
7	40–inch lines	40 miles/hour	39.6 pounds	41.0 pounds
8	40–inch lines	60 miles/hour	88.7 pounds	94.0 pounds
9	40–inch lines	80 miles/hour	157.5 pounds	– –
10	28–inch lines	40 miles/hour	– –	32.0 pounds
11	28–inch lines	40 miles/hour	– –	62.0 pounds
*The experimental model had 51–inch lines.				